Oncogenic STIL-mediated loss of BRCA1 functionality causes DNA damage and centrosome amplification

Srishti Sanghi[1] and Priyanka Singh[1*]

Author Affiliations:

[1]Department of Bioscience & Bioengineering, Indian Institute of Technology Jodhpur

NH 62, Nagaur Road, Karwar 342037, Jodhpur, Rajasthan, India.

[*]Correspondence to: priyankasingh@iitj.ac.in

Running title: Oncogenic STIL causes loss of BRCA1 functionality

SUMMARY

Centrosomes are major microtubule organizing centers in many animal cells and could also act as a communicator between nuclear-cytoplasmic signaling during DNA damages. Therefore, DNA damages cause an increase in centrosome number, however the molecular linkers remain elusive. STIL (SCL/TAL1 Interrupting locus) is a core centrosome organizing protein, which is overexpressed in different cancer types. In this work, we identify a frequently reported heterozygous missense mutation in STIL, which maps to its N-terminal located CR1 region (S76L). The oncogenic STIL-S76L loses interaction with the DNA damage response protein BRCA1 and exhibits a decrease in BRCA1 nuclear localization, which causes DNA damage and enhanced centrosome number. Interestingly, exogenous BRCA1 can rescue these phenotypes of STIL-S76L, thus, establishing it as an effector for the oncogenic STIL functions. These amplified centrosomes tend to cluster in the M phase and cause pseudo bipolar spindle organization, which is a promising target for anti-cancer drugs.

KEYWORDS: STIL, BRCA1, Centrosome, Breast Cancer, Cell division

INTRODUCTION

The gene for STIL (SCL/TAL1 Interrupting locus) was first cloned from the chromosomal rearrangements in T-cell leukemia[1]. STIL is required for cell growth and proliferation, as its loss of function mutations are lethal in mice at midgestation[2,3] and zebrafish[4]. Enhanced expression of STIL is observed in different cancers[5,6] and it has been established as an oncogene[7].

STIL is a cytoplasmic protein, where it is majorly localized at centrosomes. A centrosome contains an orthogonally arranged pair of microtubule-based cylindrical structures at its core called the centrioles, which are embedded in a protein-rich matrix referred to as the pericentriolar material (PCM). Centrosome duplicates during the S-phase of the cell cycle, which involves a cartwheel-like arrangement of core centriole proteins (procentriole) adjacent to each preexisting centriole. STIL is one of the core centriole duplication factor, whose functional orthologues are SAS5 in worms[8] and ANA2 in flies[9]. Human STIL contains several conserved regions[10], which include a Proline-rich *C*onserved *R*egion (CR2, 385-499 residues) present at the N-terminal region and involved in interactions with another core centriole protein, CPAP/CENPJ[11]. An extended CR1 region (26-324 residues) is found specifically in vertebrates, but not much is understood about its involvement in STIL functioning. The middle coiled-coil region (721-748

residues) is involved in interaction with the centrosome kinase, PLK4[12] or the mitotic kinase CDK1, to regulate their centriole localization[13]. A patch of hydrophobic residues in the coiled-coil region is involved in oligomerization, which is required for *de novo* centriole organization[14]. The C-terminal region of STIL has a STAN domain (1052-1148 residues), which interacts with the centriole cartwheel spoke protein SAS6[12], and help in procentriole organization (**Figure 1A**). The C-terminal KEN box in STIL is required for promoting APC/C (Anaphase Promoting Complex/Cyclosome)-mediated protein degradation at mitotic exit[15]. Consequently, STIL depletion inhibits centriole duplication[11] and its overexpression triggers supernumerary centrioles[16].

In the 19th century, Theodor Boveri (1862-1915) postulated the involvement of extra centrosomes in developing malignant tumors[17]. Thereafter, an increase in centrosome number is found to be positively correlated with aneuploidy and chromosomal instability in different tumor types. Extra centrosomes in *Drosophila* can affect asymmetric divisions of larval neural stem cells and transplantation of such aberrant cells in the abdomen of host flies induces tumor formation[18]. Besides, amplified centrosomes are observed in many precancerous and preinvasive lesions in humans, suggesting their involvement during the early stages of tumor progression[19-23]. Due to

the ubiquitous presence of supernumerary centrosomes in different tumor types, it is now considered as one of the "hallmarks" of cancer with a potential prognostic value[24,25].

DNA damages activate nuclear ATM/ATR-dependent damage response signaling pathways. Outside the nucleus, these damage response proteins are reported at centrosomes, making it a platform for crosstalk between nuclear-cytoplasmic signaling. The breast and ovarian cancer susceptibility gene, BRCA1 (Breast cancer gene 1) is a tumor suppressor, which binds to DNA. During the S-phase, BRCA1 displays nuclear puncta, which represent different nuclear complexes involved in protecting stalled DNA replication forks from degradation[26], silencing of inactive X-chromosome[27], chromatin modifications and epigenetic silencing[28] under different conditions,. BRCA1 contains a RING domain at the N-terminal and two tandem BRCT domains at the C-terminus region. BRCA1 and BARD1 (BRCA1-associated RING domain protein 1) heterodimerizes through their respective RING domains. The stable complex of BRCA1-BARD1 interacts with other accessory proteins for DNA damage repair[29] by homologous recombination[30] and centrosome regulation[31-34]. BRCA1 can shuttle between the nucleus and cytoplasm to carry such diverse cellular activities. The BRCT regions of BRCA1 are also required for its localization at centrosomes[35], where it interacts with γ-tubulin. BRCA1-dependent ubiquitination of γ-tubulin inhibits centrosome aster formation at the S-phase[36]. However, in the M-phase of the cell cycle,

Aurora-A/B kinase-mediated phosphorylation of BRCA1 inhibits its ubiquitination activity[37] thus allowing microtubule nucleation. BRCA1 mutations which cause loss of functionality exhibit centrosome amplification, however, it is still unclear whether the BRCA1-mediated ubiquitin ligase or the nuclear signaling regulates centrosome duplication in such cases. The BRCT domain of BRCA1 recognizes and binds to its interactors *via* a unique S-X-X-F motif, where Serine (S) is phosphorylated[38]. This motif has been identified in DNA double-strand repair proteins, Abraxas-Rap80[39], BRIP1 (BACH1/FANC)[40], and CtIP[41]. BRCA1 can also interact with the core centrosome protein STIL[42], but not much is understood about the interplay between STIL and BRCA1.

This work provides evidence that STIL and BRCA1 cross-talk with each other to maintain DNA integrity, which in turn regulates centrosome number. The STIL-BRCA1 axis is found to be disrupted in cancer patients.

RESULTS

Identification of STIL S76L oncogenic mutation in the CR1 region.

We analyzed pan-cancer mutations in *STIL* gene available on public databases, including Cancer Genome Atlas (TCGA) (https://www.cancer.gov/tcga), Catalogue Of Somatic Mutations In

Cancer (COSMIC)[43], and International Cancer Genome Consortium (ICGC)[44]. We found that 45% of cancer-associated mutations in STIL are missense. The CR1 region was found to be frequently mutated, with a total of 141 reported mutations (20%) (**Figure 1B**). The expression of EGFP tagged STIL (EGFP-STIL, 1-1287 residues) in breast cancer cells, MCF7, resulted in only a subtle increase (2.5 folds) in a population of cells with centrosome amplification (>2 γ-tubulin foci) as scored using the pericentriolar marker, γ-tubulin in prophase cells (**Figure 1C-D)**. However, the expression of the N-terminal of STIL (1-619 residues) caused a 7.6-fold increase in cell population with amplified centrosomes, which is even more as compared to the C-terminal region (5.5 folds) of STIL encompassing 619-1287 residues. This corroborates the bioinformatics analysis and suggests an important role of the STIL N-terminal region in regulating its functionality. Further analysis of CR1-associated cancer mutations led us to narrow down a frequently reported missense mutation, which changes the serine residues at 76th position to leucine (S76L). The heterozygous STIL-S76L was reported in different epithelial cancer types, including, skin, stomach, colon, and endometrial cancer (**Figure 1B and 2A)**.

Heterozygous oncogenic STIL S76L mutation causes centrosome amplification and increases cell migration

The expression of EGFP-STIL-S76L in the MCF7 cells, resulted in a significant (70.8%) population of prophase cells with amplified centrioles (>4 centrin-1 foci; a distal centriole marker), compared to control cells expressing only EGFP (**Figure 2B-C**). Centriole duplicates at S-phase of the cell cycle, so S-phase synchronized cells expressing EGFP-STIL-S67L already show a significant population (51%) with amplified centrosomes (>4 centrin-1 foci) (**Figure 2D-F**). This suggests that S76L mutation affects the centriole duplication function of STIL protein. Next, we performed a scratch assay to analyze cell migration, which is linked with tumorigenesis[45]. The MCF7 cells expressing EGFP-STIL-S76L closed the scratch by 84.5% in 48 hrs, whereas as in control (EGFP expressing cells) only 47% scratch closure was observed (**Figure 2G-H)**. This suggests that the identified STIL-associated cancerous mutation *i.e.*, S76L can impart cancerous phenotypes to dividing cells.

STIL S76L disrupts interaction with BRCA1

Close analysis of the surrounding residues of S76 (^{76}SSCF^{79}) suggested that it could be a putative BRCA1 recognition motif [38], *i.e.* S-X-X-F (**Figure 3A**). We show that endogenous STIL and BRCA1 are part of the same complex by immunoprecipitation (**Figure 3B**). Although BRCA1 is majorly a nuclear protein, it also co-localizes with STIL at centrosomes during the interphase

(**Figure S1A**). EGFP-STIL-S76L shows reduced interaction with exogenous FLAG-BRCA1 in the immunoprecipitation assay. We identified another putative BRCA1 recognition motif (SXXF) in CR1 at the 183rd position and generated a double mutant (S76L/S183A). The double mutant shows an additional reduction of STIL and BRCA1 interaction (**Figure 3C-D).** This suggests that S76 is a BRCA1 interaction site in STIL.

Depletion of BRCA1 by RNA interference (RNAi) (**Figure S1B**) had no effect on the localization of STIL at centrosomes (**Figure S1C**). However, we observed an increase in STIL ubiquitination, when the endogenous BRCA1 is knocked-down (**Figure 3E**). STIL-S76L and the double mutant S76L/S183A, which loses interaction with BRCA1, were also more ubiquitinated (**Figure 3F**). This suggests that the interaction with BRCA1 inhibits STIL ubiquitination. Surprisingly, the STIL S76L and the double mutant (S76L/S183A), were not able to localize at centrosomes (**Figure 3 G-H**), suggesting their indirect effect on centrosome number.

STIL-BRCA1 interaction is required for regulating centrosome number and DNA integrity

Depletion of STIL by RNAi (**Figure S1D**) resulted in a reduction of total BRCA1 protein levels (**Figure 4A**), which were rescued on expressing RNAi-resistant exogenous EGFP-STIL. The

EGFP-STIL-S76L, which loses BRCA1 interaction, was also able to rescue BRCA1 protein levels in the absence of endogenous STIL (**Figure 4B**). This suggests that STIL is required for BRCA1 protein stability, however, the effect of STIL on BRCA1 is independent of their interaction. Subsequently, we also observed a reduction in the number of BRCA1 nuclear foci on STIL depletion (**Figure 4C-D**). BRCA1 is exported out of the nucleus during DNA damage[46]. We performed a comet assay, which revealed that STIL or BRCA1 RNAi causes significant DNA damage compared to control cells, as scored by the percentage of DNA in the comet tail (**Figure 4E-F**). To establish a link between DNA damage and centrosome amplification, we exposed cells to UV, which resulted in 55% of S-phase cells with amplified centrosome number (>4 centrin-1 foci). The BRCA1 depletion resulting in enhanced DNA damage, also caused a significant population of S-phase cells (27.4%) with amplified centrosomes (>4 centrin-1 foci) (**Figure 5A-B**). However, centrosome amplification was not observed for STIL RNAi (**Figure S1E-F**), which also causes DNA damage, possibly because it is also one of the core proteins required for centriole assembly.

BRCA1 is the effector of oncogenic STIL-S76L phenotypes

The overexpression of exogenous EGFP-STIL-S76L in cells, expressing endogenous STIL, hereby mimicking a heterozygous condition, showed a decrease in the number of BRCA1 nuclear

foci (**Figure 5C-D**), without any effect on the total BRCA1 protein levels (**Figure 5E**). Since the reduction in BRCA1 nuclear foci signals caused DNA damages (**Figure 4 C-F**), accordingly, we observed enhanced DNA damage in the comet assay for cells expressing EGFP-STIL-S76L. Interestingly, the DNA damage can be rescued in these cells on expression of exogenous FLAG-BRCA1 (**Figure 6A-B**). The amplified centrosome phenotype observed in cells expressing EGFP-STIL-S76L or the double mutant (S76L/S183A), could also be rescued on overexpression of FLAG-BRCA1 (**Figure 6C-D**). This suggests that BRCA1 is a downstream effector for STIL-dependent regulation of centrosome number and DNA integrity.

Despite, multiple centrosomes, in STIL-S76L expressing cells multipolar spindles were not apparent, due to an increase in the cell population (62.7%) with centrosome clustering and pseudo bipolar spindle organization (**Figure 7A-B**).

DISCUSSION

STIL is a core centrosome organizing protein, which is also overexpressed in many cancer types. However, not much is understood about the mechanism by which STIL mediate cancer development. In this work, we identified a BRCA1-mediated pathway for the STIL-dependent regulation of centrosome number and DNA integrity. We show that the N-terminal region of STIL

encompasses frequently reported cancer mutations. This work led us toward the identification of an oncogenic heterozygous missense mutation, which changes serine at the 76th position to leucine (S67L). We show that S76L expression in breast cancer cells enhances centrosome numbers as observed in fluorescence microscopy and cell migration in scratch assay. Hereby confirming the oncogenic impact of the S76L mutant. The S76 residue was found to be involved in interaction with the tumor suppressor protein BRCA1 using immunoprecipitation. STIL could localize at centrosomes in the absence of BRCA1, however, enhanced ubiquitination of STIL was noted. Therefore, BRCA1 does not affect the localization of STIL at centrosomes but was found to be affect the ubiquitination status of STIL. On the other hand, STIL depletion affects BRCA1 protein stability, which reduces levels of BRCA1 in nucleus subsequently causing DNA damage. Since BRCA1 loss from the nucleus enhances DNA damage, which cause supernumerary centrosomes. We show that STIL-S76L affects centrosome number indirectly through the reduction of BRCA1 nuclear localization. Accordingly, expression of exogenous FLAG-BRCA1 in STIL-S76L expressing cells was able to rescue DNA damages and centrosome number in cells. It would be interesting to further investigate the significance of STIL ubiquitination and its correlation to DNA damage. We show that the STIL-BRCA1 interaction is important for protecting cells from DNA damage, which can further impact the number the centrosomes. (**Figure 7C**). The cells expressing

STIL-S76L shows centrosome clustering and pseudo bipolar spindles, which is a promising therapeutic target for small molecule inhibitors[47]. This work reports a novel STIL-BRCA1 axis, which opens new possibilities of chemo-therapeutic interventions for cancer.

MATERIAL & METHODS

Cell Culture and Synchronization

MCF7 cells were maintained in Dulbecco's modified Eagle's medium (Himedia#Al111) supplemented with 1% L-glutamine, 1% Pen/Strep and 10% fetal bovine serum (Himedia #RM10434,). Cells were synchronized in S phase using a double-thymidine block[48]. Briefly, cells were incubated with 2 mM thymidine (Sigma# T9250) for 18 hrs, followed by a 9 hrs of release, and the second block was introduced for 15 hrs followed by harvesting. For M-phase, cells were synchronized using a double-thymidine block followed by a 12 hrs release.

siRNA, Plasmids and Transfection

Double-stranded STIL siRNA and BRCA1 siRNA oligonucleotides were synthesized (Biotech Desk Pvt Ltd) with 3'-UU overhangs with the following sense strand sequences, 5'-GUUUAAGGGAAAAGUUAUU-3'[49] and 5'-CAGGAAAUGGCUGAACUAGAA-3'[50], respectively. siRNA (72 nM) was transfected using Lipofectamine 3000 reagent as per the

manufacturer's protocol (Invitrogen #L3000001). The pcDNA5 FRT/TO MycLAP-STIL plasmids was ordered from Addgene (#80266). The pcDNA5 FRT/TO/EGFP plasmids is a gift from the laboratory of Prof. Andrew Mussachio. pcDNA5 FRT/TO MycLAP-STIL_S76L and pcDNA5 FRT/TO MycLAP-STIL_S76L_S183A were generated using site-directed mutagenesis, using primers 5'-CAGAATAAAAAAAATTTGTCATGCTTTTTACTT-3' and 5'-GAGAGTTTGGACGCTGTGGAATTT-3' respectively. pDEST 3xFlag-pcDNA5-FRT/TO-BRCA1 was ordered from Addgene (#52504) Plasmids were transfected using Polyethylenimine Max[51] (Polysciences #23966-100).

Primary & Secondary antibodies

Following primary antibodies for immunofluorescence (IF) and western blotting (WB) with indicated dilution were used: mouse anti-γ tubulin antibody (Sigma #T5326, 1:100 IF), rabbit anti-Centrin-1 antibody (Abcam#ab101332, 1:500 IF), mouse anti-Centrin-1 20H5 antibody (Merck Millipore#04-1624, 1:200 IF), mouse anti-α tubulin antibody (Sigma#T9026, 1:100 IF, 1:1000 WB), mouse anti-BRCA1 D-9 antibody (Santa Cruz Biotechnology#SC6954, 1:100 IF, 1:1000 WB), rabbit anti-STIL antibody (Abcam#ab89314, 1:50 IF, 1:2000 WB), rabbit anti-ubiquitin antibody (Abcam#ab134953, 1:2000 WB) and rabbit anti-GFP antibody (Sigma #G1544, 1:7000

WB). Following secondary antibodies at the indicated dilution were used for IF: Anti-rabbit IgG (Fc) TRITC (Sigma #SAB3700846, 1:500), Anti-mouse IgG (Fc) TRITC (Sigma #SAB3701020, 1:500), Anti-rabbit IgG FITC (Sigma #F7512, 1:750), Anti-mouse IgG FITC (Sigma #F5387, 1:750). Following secondary antibodies at the indicated dilution were used for WB: Anti-mouse IgG HRP antibody (Cell Signaling Technology #7076S, 1:10000) and anti-rabbit IgG HRP (Cell Signaling Technology #7074S, 1:10000).

Immunofluorescence Microscopy

Cells were seeded on a poly-D-lysine hydrobromide (P7280, Sigma) coated 12 mm coverslips. They were permeabilized for 2 minutes using 0.1% Triton X in 1X PBS and fixed using 4% paraformaldehyde for 10 minutes. After three washes with 1X PBS, blocking solution (1% BSA in PBS + 0.1% Tween 20) was added for 1 hr. Primary antibodies were diluted in blocking solution and the coverslips were kept at 4˚C overnight. This was followed by three washes with 1X PBS and incubation with secondary antibody solutions for 1 hr at room temperature. After three washes with 1X PBS, 0.5μg/ml DAPI in 1X PBS was added to the cells for 10 minutes in the dark to stain nucleus. The coverslips were mounted onto a glass slide using DABCO-Mowiol mounting media and stored at 4˚C. Fluorescence images were taken using an Olympus IX83

fluorescence microscope with 100X oil, 1.35 NA objective lens. The images were analyzed using the ImageJ software.

Immunoprecipitation and Western blotting

Cells were suspended in ice cold RIPA buffer (150mM NaCl, 5mM EDTA pH 8, 50mM Tris pH 8, 1% NP40, 0.5% sodium deoxycholate, 0.1% SDS) supplemented with 0.5% protease and phosphatase inhibitors and lysed by passing through a small syringe needle. Lysates were cleared by centrifugation at 14,500xg for 30 minutes. Cell lysate was incubated with anti-STIL antibody (1:50) or anti-GFP antibody (1:200) overnight at 4˚C. Protein G-sepharose beads were added to the lysate-antibody mixture for 4 hours at 4˚C on shaking. Beads were washed with 1X RIPA thrice at 300xg for 2 minutes. The protein complex was eluted in the Laemmli sample buffer and resolved on 10% polyacrylamide gels. For western blotting, resolved protein bands from SDS-PAGE were transferred to the nitrocellulose membrane. Membrane was blocked using 5% BSA in 1xPBST (1X PBS with 0.05% Tween-20) for 1 hr and incubated with primary antibody at 4˚C for overnight. The membrane was washed with 1X PBST thrice and incubated with the HRP-conjugated secondary antibody for 1 hour at room temperature. The blot was developed using

Clarity Western ECL substrate (Biorad #1705061) for 5 minutes in the dark and analyzed using gel documentation system (Biotron Omega Lum G).

Cell Migration Assay

MCF7 cells at 50% confluency were transfected with EGFP-STIL constructs. At 70% confluency, the cells were given a media change to serum free DMEM. Using a pipette tip, the monolayer was scratched at nine different reference points and images were taken at 0 hr, 24 hrs and 48 hrs time points using the Olympus IX83 fluorescence microscope with a 20X dry objective[52]. Images were analyzed using the Wound Healing Size ImageJ plugin[53]. The percentage wound closure was calculated as follows -

$$\text{Wound Closure\%} = [(A_0 - A_{\Delta t}))/A_0] \times 100$$

Where, A_0 is the initial wound area, $A_{\Delta t}$ is the wound area after n hours of the initial scratch.

Ubiquitination Assay

MCF7 cells were transfected with STIL constructs and synchronized using double thymidine block. 5μM MG-132 was added to the cells for 16 hours before lysis. Cells were lysed in RIPA buffer supplemented with 0.5% protease and phosphatase inhibitors and 10 mM N-ethylmaleimide. Immunoprecipitation was performed as described above using the STIL primary

antibody. Protein complexes were blotted on a nitrocellulose membrane and incubated with rabbit anti-ubiquitin primary antibody (Abcam # ab134953) to look at protein ubiquitination in a western blot.

Comet Assay

Agarose coated slides were prepared by dipping in 1% agarose solution in 1X PBS. In case of UV exposure condition, the MCF7 cells were exposed to UVC for 30 minutes. For endogenous DNA damage, MCF7 cells were transfected with the indicated plasmid constructs for 48 hrs and 2 X 10^5 cells/ml were added to a 24 well plate. 1 ml of 1% Low Melting Point agarose solution in 1X PBS was added to each well and mixed with cells gently. The mixture was overlaid on agarose coated slides on ice and kept for 15 minutes. All steps post this were performed in the dark. The slides were incubated in the lysis buffer (2.5M NaCl, 100mM EDTA, 10mM Tris, 200mM NaOH at pH 10.5, 1% Triton-X100 and 1% DMSO) on ice for 2 hours. Subsequently, the slides were incubated in cold electrophoresis buffer (300mM NaOH, 1mM EDTA, 1% DMSO at pH > 13) for 30 minutes. Slides were shifted to an electrophoresis chamber and run at 21V for 30 minutes. After two washes with distilled water, the slides were stained using 2.5 mg/ml Propidium iodide solution. Excess of stained was washed with distilled water and the slides were

dried overnight at room temperature. The images were captures using a 10X objective of the Olympus IX83 fluorescence microscope. DNA damage was assessed using the OpenComet plugin available for ImageJ[54].

Centriole counting and Fluorescence Intensity Quantification

Centrin-1 was used as a centriolar marker in for the centriole counting. The number of centrin-1 dots were counted for each cell and the number of cells with 4 or >4 centrioles were scored. The percentage of cells with 4 or >4 centrioles was calculated by dividing with the total number of cells. The mean percentage±SEM was calculated from 2-3 independent experiments.

For intensity measurements, Centrin-1 signal was used as a reference to draw a region of interest (ROI) in ImageJ[55]. The same ROI was duplicated into the EGFP channel. The same size ROI was also placed around the centrosome to measure the background. The absolute fluorescence intensity of EGFP was reported after subtracting the average background signal of the same channel.

Statistical analysis and Softwares

All bar graphs were generated in Microsoft Excel, which plots the mean absolute fluorescence intensity±SEM. Experiments were repeated at least twice, and the number of cells (n) analyzed

was >50 for each experiment. For intensity measurements, the p-value was calculated using a two-tailed Student's t-test with unequal variance for the two conditions as indicated on top of bar graphs using a solid line. The p-values for centriole and spindle pole counting experiments were calculated using the chi-square test. Figure panels were arranged on Microsoft PowerPoint.

DATA AVAILABILITY

This study includes no data deposited in external repositories

ACKNOWLEDGEMENTS

The pcDNA5 FRT/TO/EGFP plasmids is a gift from the laboratory of Prof. Andrew Mussachio. We thank the Centre for Research & Development of Scientific Instruments at IIT Jodhpur for the microscopy facility.

FUNDING

The work is supported by the grants received from the Board of Research in Nuclear Sciences (55/14/02/2021-BRNS/10206) and the Department of Biotechnology (BT/12/IYBA/2019/02)

DISCLOSURE & COMPETING INTERESTS STATEMENT

The authors declare no competing or financial interests.

AUTHOR CONTRIBUTIONS

Conceptualization: S.S., P.S.; Methodology: S.S.; Validation: S.S., P.S.; Formal analysis: S.S., P.S.; Investigation: S.S.; Data curation: S.S., P.S.; Writing original draft: S.S. P.S.; Writing-review & editing: P.S.; Supervision: P.S.; Project administration: P.S.; Funding acquisition: P.S.

REFERENCES

1. Aplan, P.D., Lombardi, D.P., Ginsberg, A.M., Cossman, J., Bertness, V.L., and Kirsch, I.R. (1990). Disruption of the Human SCL Locus by "Illegitimate" V-(D)-J Recombinase Activity. Science *250*, 1426-1429. 10.1126/science.2255914.

2. Izraeli, S., Lowe, L.A., Bertness, V.L., Good, D.J., Dorward, D.W., Kirsch, I.R., and Kuehn, M.R. (1999). The SIL gene is required for mouse embryonic axial development and left-right specification. Nature *399*, 691-694. 10.1038/21429.

3. David, A., Liu, F., Tibelius, A., Vulprecht, J., Wald, D., Rothermel, U., Ohana, R., Seitel, A., Metzger, J., Ashery-Padan, R., et al. (2014). Lack of centrioles and primary cilia in STIL−/− mouse embryos. Cell Cycle *13*, 2859-2868. 10.4161/15384101.2014.946830.

4. Pfaff, K.L., Straub, C.T., Chiang, K., Bear, D.M., Zhou, Y., and Zon, L.I. (2007). The Zebra fish cassiopeia Mutant Reveals that SIL Is Required for Mitotic Spindle Organization. Mol Cell Biol *27*, 5887-5897. 10.1128/MCB.00175-07.

5. Erez, A., Perelman, M., Hewitt, S.M., Cojacaru, G., Goldberg, I., Shahar, I., Yaron, P., Muler, I., Campaner, S., Amariglio, N., et al. (2004). Sil overexpression in lung cancer characterizes tumors with increased mitotic activity. Oncogene *23*, 5371-5377. 10.1038/sj.onc.1207685.

6. Ouyang, Y., Jin, Y.B., Chen, X.P., Zhang, G.Y., Mao, S.L., Ling, F., and Luo, W. (2020). STIL is upregulated in nasopharyngeal carcinoma tissues and promotes nasopharyngeal carcinoma proliferation, migration and invasion. Neoplasma *67*, 37-45. 10.4149/neo_2019_190306N192.

7. Li, J., Yang, Z., Qi, Y., Liu, X., Liu, Y., Gao, X., Li, S., Zhu, J., Zhang, C., Du, E., et al. (2022). STIL Acts as an Oncogenetic Driver in a Primary Cilia-Dependent Manner in Human Cancer. Front Cell Dev Biol *10*, 10:804419. 10.3389/fcell.2022.804419.

8. Delattre, M., Canard, C., and Gönczy, P. (2006). Sequential protein recruitment in C. elegans centriole formation. Curr Biol *16*, 1844-1849. 10.1016/j.cub.2006.07.059.

9. Stevens, N.R., Roque, H., and Raff, J.W. (2010). DSas-6 and Ana2 Coassemble into Tubules to Promote Centriole Duplication and Engagement. Dev Cell *19*, 913-919. 10.1016/j.devcel.2010.11.010.

10. Patwardhan, D., Mani, S., Passemard, S., Gressens, P., and El Ghouzzi, V. (2018). STIL balancing primary microcephaly and cancer. Cell Death Dis *9*, 65. 10.1038/s41419-017-0101-9.

11. Tang, C.-J.C., Lin, S.-Y., Hsu, W.-B., Lin, Y.-N., Wu, C.-T., Lin, Y.-C., Chang, C.-W., Wu, K.-S., and Tang, T.K. (2011). The human microcephaly protein STIL interacts with CPAP and is required for procentriole formation. EMBO J *30*, 4790-4804. 10.1038/emboj.2011.378.

12. Ohta, M., Ashikawa, T., Nozaki, Y., Kozuka-Hata, H., Goto, H., Inagaki, M., Oyama, M., and Kitagawa, D. (2014). Direct interaction of Plk4 with STIL ensures formation of a single procentriole per parental centriole. Nat Commun *5*, 5267. 10.1038/ncomms6267.

13. Zitouni, S., Francia, M.E., Leal, F., Gouveia, S.M., Nabais, C., Duarte, P., Gilberto, S., Brito, D., Moyer, T., Kandels-Lewis, S., et al. (2016). CDK1 prevents unscheduled PLK4-STIL complex assembly in centriole biogenesis. Curr Biol *26*, 1127-1137. 10.1016/j.cub.2016.03.055.

14. David, A., Amartely, H., Rabinowicz, N., Shamir, M., Friedler, A., and Izraeli, S. (2016). Molecular basis of the STIL coiled coil oligomerization explains its requirement for de-novo formation of centrosomes in mammalian cells. Sci Rep *6*, 24296. 10.1038/srep24296.

15. Arquint, C., and Nigg, E.A. (2014). STIL microcephaly mutations interfere with APC/C-mediated degradation and cause centriole amplification. Curr Biol *24*, 351-360. 10.1016/j.cub.2013.12.016.

16. Arquint, C., Sonnen, K.F., Stierhof, Y.-D., and Nigg, E.A. (2012). Cell-cycle-regulated expression of STIL controls centriole number in human cells. J Cell Sci *125*, 1342-1352. 10.1242/jcs.099887.

17. Boveri, T. (2008). Concerning the Origin of Malignant Tumours by Theodor Boveri. Translated and annotated by Henry Harris. J Cell Sci *121*, 1-84. 10.1242/jcs.025742.

18. Basto, R., Brunk, K., Vinadogrova, T., Peel, N., Franz, A., Khodjakov, A., and Raff, J.W. (2008). Centrosome Amplification Can Initiate Tumorigenesis in Flies. Cell *133*, 1032-1042. 10.1016/j.cell.2008.05.039.

19. Chng, W.J., Ahmann, G.J., Henderson, K., Santana-Davila, R., Greipp, P.R., Gertz, M.A., Lacy, M.Q., Dispenzieri, A., Kumar, S., Rajkumar, S.V., et al. (2006). Clinical implication of centrosome amplification in plasma cell neoplasm. Blood *107*, 3669-3675. 10.1182/blood-2005-09-3810.

20. Pihan, G.A., Wallace, J., Zhou, Y., and Doxsey, S.J. (2003). Centrosome abnormalities and chromosome instability occur together in pre-invasive carcinomas. Cancer Res *63*, 1398-1404.

21. Kayser, G., Gerlach, U., Walch, A., Nitschke, R., Haxelmans, S., Kayser, K., Hopt, U., Werner, M., and Lassmann, S. (2005). Numerical and structural centrosome aberrations are an early and stable event in the adenoma-carcinoma sequence of colorectal carcinomas. Virchows Arch *447*, 61-65. 10.1007/s00428-004-1191-1.

22. Hsu, L.-C., Kapali, M., DeLoia, J.A., and Gallion, H.H. (2005). Centrosome abnormalities in ovarian cancer. Int J Cancer *113*, 746-751. 10.1002/ijc.20633.

23. Kronenwett, U., Huwendiek, S., Castro, J., Ried, T., and Auer, G. (2005). Characterisation of breast fine-needle aspiration biopsies by centrosome aberrations and genomic instability. Br J Cancer *92*, 389-395. 10.1038/sj.bjc.6602246.

24. Mittal, K., Kaur, J., Jaczko, M., Wei, G., Toss, Michael.S., Rakha, E.A., Janssen, E.A.M., Søiland, H., Kucuk, O., Reid, M.D., et al. (2021). Centrosome amplification: a quantifiable cancer cell trait with prognostic value in solid malignancies. Cancer Metastasis Rev *40*, 319-339. 10.1007/s10555-020-09937-z.

25. Chan, J.Y. (2011). A Clinical Overview of Centrosome Amplification in Human Cancers. Int J Biol Sci *7*, 1122-1144. 10.7150/ijbs.7.1122.

26. Schlacher, K., Wu, H., and Jasin, M. (2012). A Distinct Replication Fork Protection Pathway Connects Fanconi Anemia Tumor Suppressors to RAD51-BRCA1/2. Cancer Cell *22*, 106-116. 10.1016/j.ccr.2012.05.015.

27. Ganesan, S., Silver, D.P., Greenberg, R.A., Avni, D., Drapkin, R., Miron, A., Mok, S.C., Randrianarison, V., Brodie, S., Salstrom, J., et al. (2002). BRCA1 supports XIST RNA concentration on the inactive X chromosome. Cell *111*, 393-405. 10.1016/s0092-8674(02)01052-8.

28. Henderson, B.R. (2012). The BRCA1 Breast Cancer Suppressor: Regulation of Transport, Dynamics, and Function at Multiple Subcellular Locations. Scientifica (Cairo) *2012*, 796808. 10.6064/2012/796808.

29. Tarsounas, M., and Sung, P. (2020). The antitumorigenic roles of BRCA1-BARD1 in DNA repair and replication. Nat Rev Mol Cell Biol *21*, 284-299. 10.1038/s41580-020-0218-z.

30. Zhao, W., Wiese, C., Kwon, Y., Hromas, R., and Sung, P. (2019). The BRCA Tumor Suppressor Network in Chromosome Damage Repair by Homologous Recombination. Annu. Rev. Biochem. *88*, 221-245. 10.1146/annurev-biochem-013118-111058.

31. Matsuzawa, A., Kanno, S., Nakayama, M., Mochiduki, H., Wei, L., Shimaoka, T., Furukawa, Y., Kato, K., Shibata, S., Yasui, A., et al. (2014). The BRCA1/BARD1-Interacting Protein OLA1 Functions in Centrosome Regulation. Mol Cell *53*, 101-114. 10.1016/j.molcel.2013.10.028.

32. Starita, L.M., Machida, Y., Sankaran, S., Elias, J.E., Griffin, K., Schlegel, B.P., Gygi, S.P., and Parvin, J.D. (2004). BRCA1-Dependent Ubiquitination of γ-Tubulin Regulates Centrosome Number. Mol Cell Biol *24*, 8457-8466. 10.1128/MCB.24.19.8457-8466.2004.

33. Yoshino, Y., Qi, H., Fujita, H., Shirota, M., Abe, S., Komiyama, Y., Shindo, K., Nakayama, M., Matsuzawa, A., Kobayashi, A., et al. (2018). BRCA1-Interacting Protein OLA1 Requires Interaction with BARD1 to Regulate Centrosome Number. Mol Cancer Res *16*, 1499-1511. 10.1158/1541-7786.MCR-18-0269.

34. Yoshino, Y., Qi, H., Kanazawa, R., Sugamata, M., Suzuki, K., Kobayashi, A., Shindo, K., Matsuzawa, A., Shibata, S., Endo, S., et al. (2019). RACK1 regulates centriole duplication by controlling localization of BRCA1 to the centrosome in mammary tissue-derived cells. Oncogene *38*, 3077-3092. 10.1038/s41388-018-0647-8.

35. Hsu, L.-C., and White, R.L. (1998). BRCA1 is associated with the centrosome during mitosis. Proc. Natl. Acad. Sci. U.S.A. *95*, 12983-12988. 10.1073/pnas.95.22.12983.

36. Sankaran, S., Starita, L.M., Groen, A.C., Ko, M.J., and Parvin, J.D. (2005). Centrosomal Microtubule Nucleation Activity Is Inhibited by BRCA1-Dependent Ubiquitination. Mol Cell Biol *25*, 8656-8668. 10.1128/MCB.25.19.8656-8668.2005.

37. Sankaran, S., Crone, D.E., Palazzo, R.E., and Parvin, J.D. (2007). Aurora-A kinase regulates breast cancer associated gene 1 inhibition of centrosome-dependent microtubule nucleation. Cancer Res *67*, 11186-11194. 10.1158/0008-5472.CAN-07-2578.

38. Manke, I.A., Lowery, D.M., Nguyen, A., and Yaffe, M.B. (2003). BRCT Repeats As Phosphopeptide-Binding Modules Involved in Protein Targeting. Science *302*, 636-639. 10.1126/science.1088877.

39. Wang, B., Matsuoka, S., Ballif, B., Zhang, D., Smogorzewska, A., Giyi, S., and Elledge, S.J. (2007). Abraxas and Rap80 form a novel BRCA1 protein complex required for the DNA damage response. Science *316*, 1194-1198. 10.1126/science.1139476.

40. Yu, X., Chini, C.C.S., He, M., Mer, G., and Chen, J. (2003). The BRCT Domain Is a Phospho-Protein Binding Domain. Science *302*, 639-642. 10.1126/science.1088753.

41. Yu, X., and Chen, J. (2004). DNA Damage-Induced Cell Cycle Checkpoint Control Requires CtIP, a Phosphorylation-Dependent Binding Partner of BRCA1 C-Terminal Domains. Mol Cell Biol *24*, 9478-9486. 10.1128/MCB.24.21.9478-9486.2004.

42. Rabinowicz, N., Mangala, L.S., Brown, K.R., Checa-Rodriguez, C., Castiel, A., Moskovich, O., Zarfati, G., Trakhtenbrot, L., Levy-Barda, A., Jiang, D., et al. (2017). Targeting the centriolar replication factor STIL synergizes with DNA damaging agents for treatment of ovarian cancer. Oncotarget *8*, 27380-27392. 10.18632/oncotarget.16068.

43. Tate, J.G., Bamford, S., Jubb, H.C., Sondka, Z., Beare, D.M., Bindal, N., Boutselakis, H., Cole, C.G., Creatore, C., Dawson, E., et al. (2019). COSMIC: the Catalogue Of Somatic Mutations In Cancer. Nucleic Acids Res *47*, D941-D947. 10.1093/nar/gky1015.

44. Zhang, J., Bajari, R., Andric, D., Gerthoffert, F., Lepsa, A., Nahal-Bose, H., Stein, L.D., and Ferretti, V. (2019). The International Cancer Genome Consortium Data Portal. Nat Biotechnol *37*, 367-369. 10.1038/s41587-019-0055-9.

45. Friedl, P., and Wolf, K. (2003). Tumour-cell invasion and migration: diversity and escape mechanisms. Nat Rev Cancer *3*, 362-374. 10.1038/nrc1075.

46. Feng, Z., Kachnic, L., Zhang, J., Powell, S.N., and Xia, F. (2004). DNA damage induces p53-dependent BRCA1 nuclear export. J Biol Chem *279*, 28574-28584. 10.1074/jbc.M404137200.

47. Mariappan, A., Soni, K., Schorpp, K., Zhao, F., Minakar, A., Zheng, X., Mandad, S., Macheleidt, I., Ramani, A., Kubelka, T., et al. (2019). Inhibition of CPAP-tubulin interaction prevents proliferation of centrosome amplified cancer cells. EMBO J *38*, e99876. 10.15252/embj.201899876.

48. Chen, G., and Deng, X. (2018). Cell Synchronization by Double Thymidine Block. Bio Protoc *8*, e2994. 10.21769/BioProtoc.2994.

49. Jaiswal, S., Sanghi, S., and Singh, P. (2023). Separation-of-function MCPH-associated mutations in CPAP affect centriole number and length. J Cell Sci *136*, jcs261297. 10.1242/jcs.261297.

50. Urban, V., Dobrovolna, J., Hühn, D., Fryzelkova, J., Bartek, J., and Janscak, P. (2016). RECQ5 helicase promotes resolution of conflicts between replication and transcription in human cells. Journal of Cell Biology *214*, 401-415. 10.1083/jcb.201507099.

51. Longo, P.A., Kavran, J.M., Kim, M.-S., and Leahy, D.J. (2013). Transient Mammalian Cell Transfection with Polyethylenimine (PEI). Methods Enzymol *529*, 227-240. 10.1016/B978-0-12-418687-3.00018-5.

52. Liang, C.-C., Park, A.Y., and Guan, J.-L. (2007). In vitro scratch assay: a convenient and inexpensive method for analysis of cell migration in vitro. Nat Protoc *2*, 329-333. 10.1038/nprot.2007.30.

53. Suarez-Arnedo, A., Figueroa, F.T., Clavijo, C., Arbeláez, P., Cruz, J.C., and Muñoz-Camargo, C. (2020). An image J plugin for the high throughput image analysis of in vitro scratch wound healing assays. PLOS ONE *15*, e0232565. 10.1371/journal.pone.0232565.

54. Clementi, E., Garajova, Z., and Markkanen, E. (2021). Measuring DNA Damage Using the Alkaline Comet Assay in Cultured Cells. Bio Protoc *11*, e4119. 10.21769/BioProtoc.4119.

55. Schindelin, J., Arganda-Carreras, I., Frise, E., Kaynig, V., Longair, M., Pietzsch, T., Preibisch, S., Rueden, C., Saalfeld, S., Schmid, B., et al. (2012). Fiji - an Open Source platform for biological image analysis. Nat Methods *9*, 10.1038/nmeth.2019. 10.1038/nmeth.2019.

FIGURES

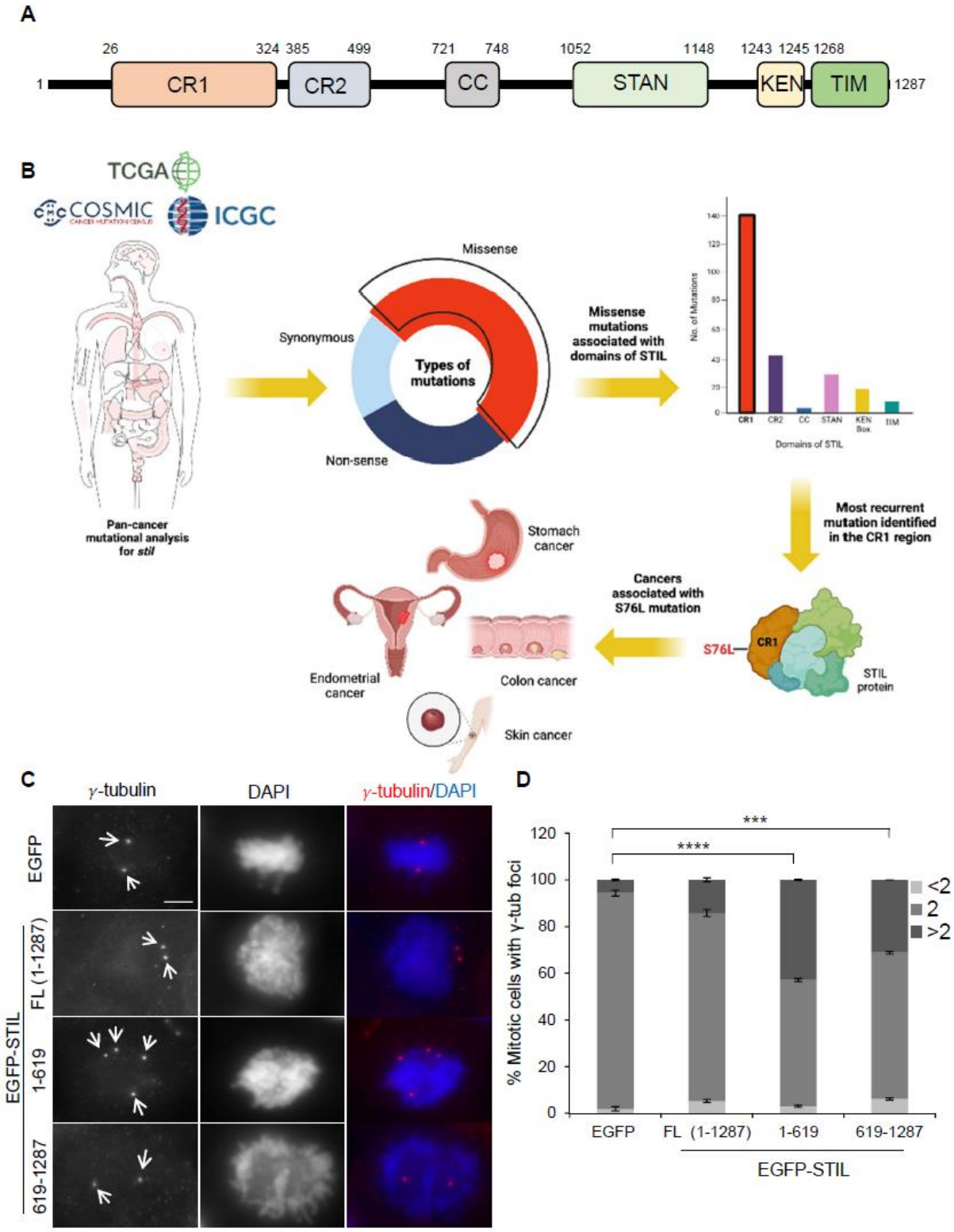
A
26
324 385
499
721
748
1052
1148
1243 1245 1268
1
CR1
CR2
CC
STAN
KEN
TIM
1287
B
TCGA
COSMIC
ICGC
Pan-cancer mutational analysis for stil
Missense
Synonymous
Types of mutations
Non-sense
Missense mutations associated with domains of STIL
No. of Mutations
CR1
CR2
CC
STAN
KEN Box
TIM
Domains of STIL
Most recurrent mutation identified in the CR1 region
S76L
CR1
STIL protein
Cancers associated with S76L mutation
Stomach cancer
Endometrial cancer
Colon cancer
Skin cancer
C
γ-tubulin
DAPI
γ-tubulin/DAPI
EGFP
EGFP-STIL
FL (1-1287)
1-619
619-1287
D
***
****
% Mitotic cells with γ-tub foci
<2
2
>2
EGFP
FL (1-1287)
1-619
619-1287
EGFP-STIL

Figure 1: STIL N-terminal region is prone to cancer-associated mutations. (A) Schematic representation of conserved regions of human STIL. Numbers indicate amino acid residues marking the position of different regions in the protein. CR1 (conserved region 1), CR2 (conserved region 2) and CC (coiled-coil). **(B)** The workflow for identification of STIL associated cancer mutation from the pan cancer datasets available in various cancer databases. Majority of missense mutations were reported in the CR1 region of STIL. **(C)** Immunofluorescence images of mitotic MCF7 cells transfected with EGFP (control) or EGFP-STIL [full-length, FL (1-1288 residues); 1-619 residues (N-terminal); 619-1288 (C-terminal)] and stained with pericentriolar marker, γ-tubulin and nuclear stain, DAPI. White arrows mark centrosomes/cell. Scale bar: 5μm. **(D)** Bar graph showing the mean percentage of mitotic cells±SEM with >2 (dark gray), 2 (medium gray) and <2 (light gray) γ-tubulin dots in the respective conditions. Results are from two independent experiments (n=50-100). ∗∗∗p<0.001 and ∗∗∗∗p<0.0001 (Chi-squared test)

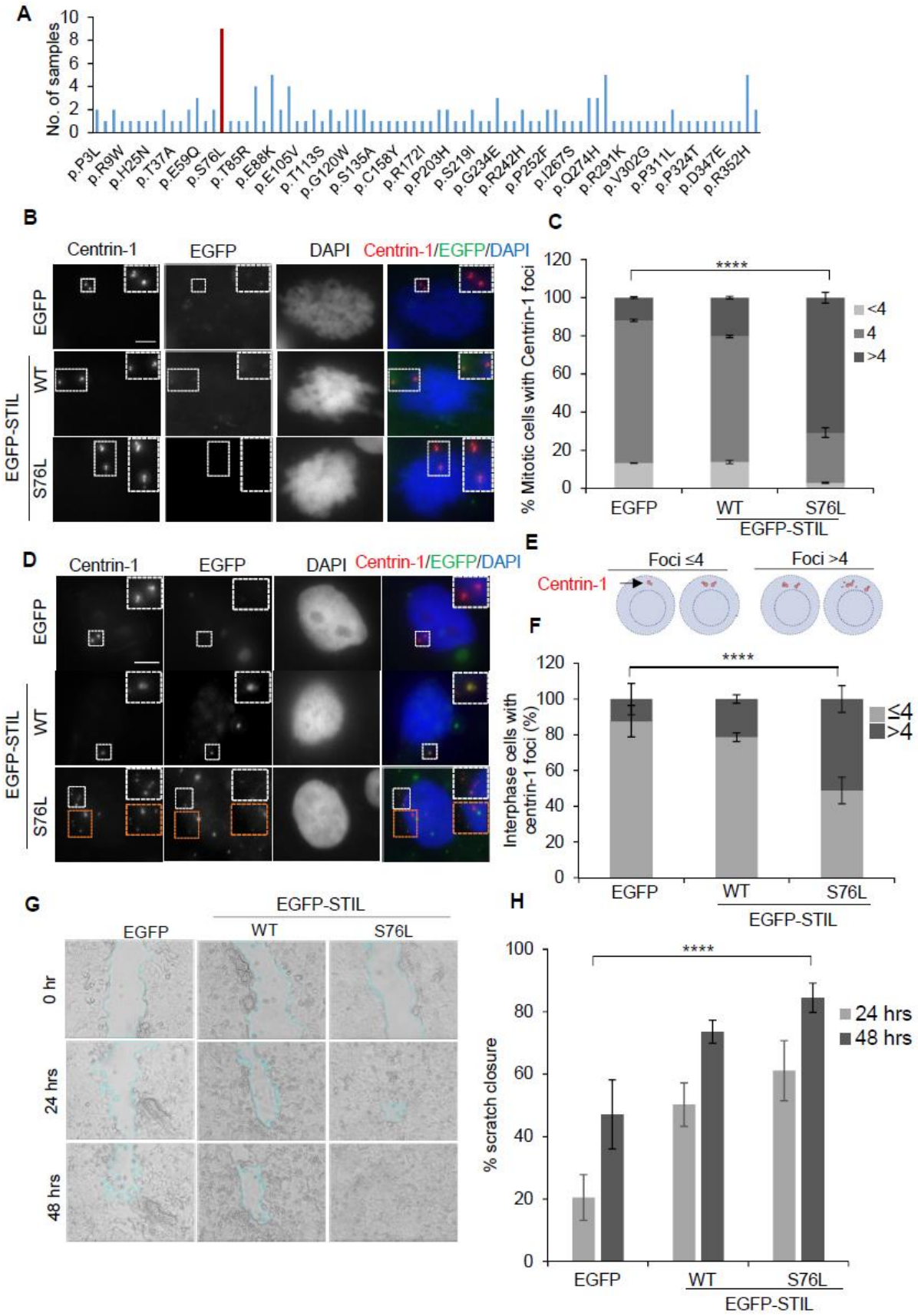
A
No. of samples
p.P3L
p.R9W
p.H25N
p.T37A
p.E59Q
p.S76L
p.T85R
p.E88K
p.E105V
p.T113S
p.G120W
p.S135A
p.C158Y
p.R172I
p.P203H
p.S219I
p.G234E
p.R242H
p.P252F
p.I267S
p.Q274H
p.R291K
p.V302G
p.P311L
p.P324T
p.D347E
p.R352H
B
Centrin-1
EGFP
DAPI
Centrin-1/EGFP/DAPI
EGFP-STIL
WT
S76L
C
% Mitotic cells with Centrin-1 foci
****
<4
4
>4
EGFP
WT
S76L
EGFP-STIL
D
E
Foci ≤4
Foci >4
Centrin-1
F
Interphase cells with centrin-1 foci (%)
≤4
>4
G
H
% scratch closure
24 hrs
48 hrs
0 hr

Figure 2: The STIL-S76L exhibits enhanced centrosome number and cell migration. (A) Bar graph represents number of reported missense mutations associated with each residue in the CR1 region of STIL. **(B)** Immunofluorescence images of mitotic MCF7 cells expressing EGFP (control) or EGFP-STIL (wild type, WT; S76L, mutant). The cells are stained with centrin-1 (centriolar marker) and DAPI (nuclear marker). Insets show a magnified view of centrioles. Scale bar: 5μm. **(C)** Bar graph showing the mean percentage of mitotic cells±SEM with >4 (dark gray), 4 (medium gray) and <4 (light gray) centrin-1 dots in the respective conditions in (B). Results are average from three independent experiments (n=50-100). ∗∗∗∗p<0.0001 (Chi-squared test). **(D)** Immunofluorescence images of S-phase synchronized MCF7 cells expressing EGFP (control) or EGFP-STIL (wild type, WT; S76L, mutant). The cells were stained with centrin-1 (centriole marker) and DAPI (nuclear marker). Insets show a magnified view of centrioles. Scale bar: 5μm. **(E)** Cartoon depicting interphase cells scored under □4 or >4 centrin-1 foci. **(F)** Bar graph showing the mean percentage of interphase cells±SEM. with >4 (dark gray) and □4 (light gray) centrin-1 foci for the respective conditions in (D). Results are from two independent experiments (n=100-180). ∗∗∗∗p<0.0001 (Chi-squared test). **(G)** Bright field images showing scratch closure at 0 hr, 24 hrs and 48 hrs in MCF7 cells transfected with EGFP (control) or EGFP-STIL

(wild type, WT; S76L, mutant). (**H**) Bar graph showing mean percentage of scratch closure±SEM at 24 hrs (light gray) and 48 hrs (dark gray) for conditions in (G). Results are from two

independent experiments. ****p<0.0001 (two-tailed unpaired Student's t-test).

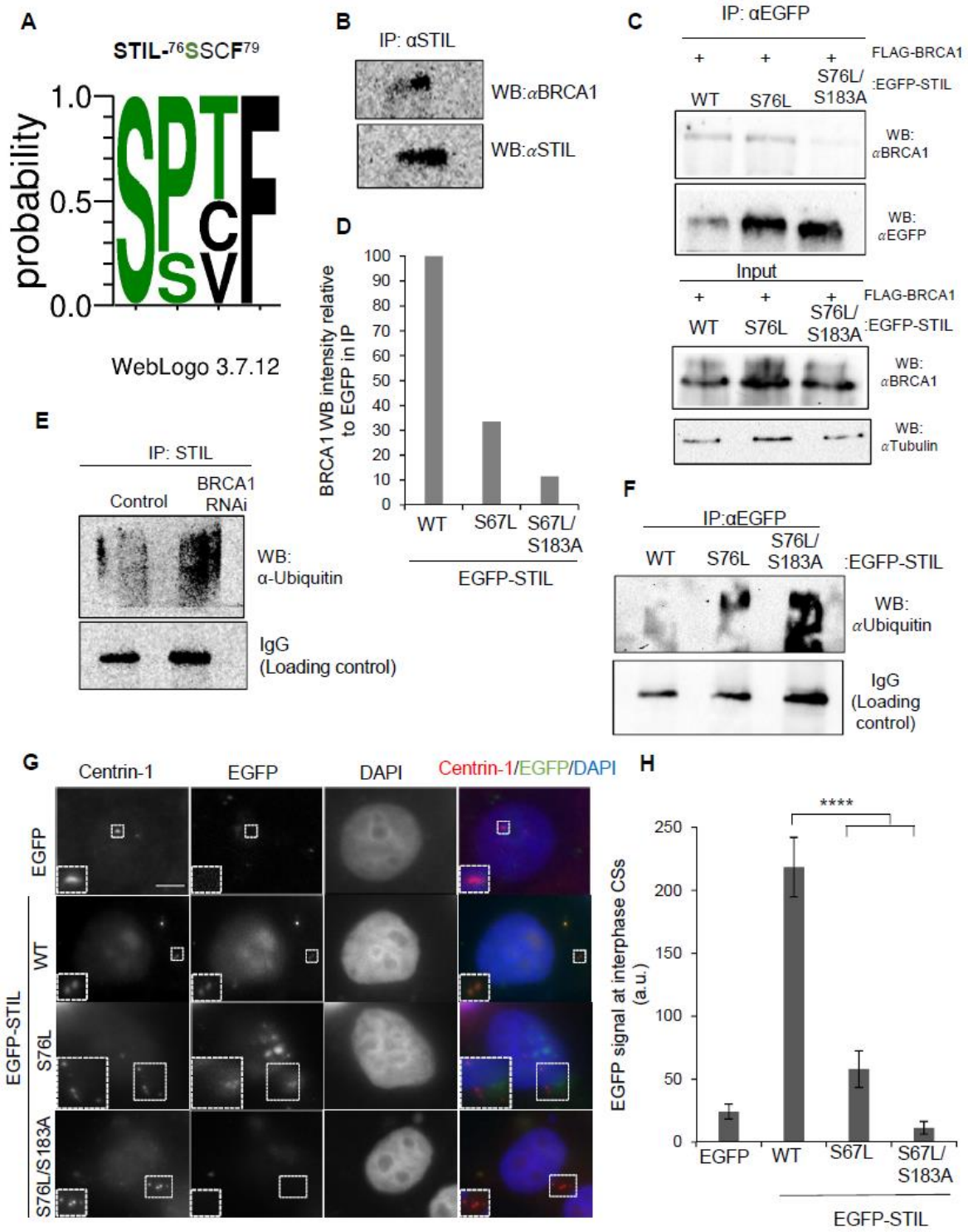

Figure 3: STIL-S76L disrupts interaction with BRCA1. (**A**) Probability index for residues in the BRCA1 recognition motif *i.e.,* SXXF. Created using Weblogo version 3.7.12. (**B**) Western blot showing immunoprecipitation of endogenous STIL from MCF7 cells, developed using STIL and BRCA1 antibodies. The blot is representation of two repeats. (**C**) Western blot shows immunoprecipitation (IP) using EGFP antibody from MCF7 cells expressing FLAG-BRCA1 and EGFP_STIL (Wild type, WT; S76L mutant, S76L/S183A double mutant). The blot is developed using BRCA1 and EGFP antibodies. The input lanes were developed using α-tubulin antibody, which indicate BRCA1 loading control. The blot is representation of two repeats. (**D**) The bar graph shows relative levels of BRCA1 normalized against EGFP bands in the IP blot from (C). The band intensity was calculated in ImageJ. (**E**) Western blot showing ubiquitination levels of immunoprecipitated (IP) endogenous STIL in control *vs*. BRCA1 depletion (RNAi) condition. IgG bands serve as loading control. The blot is representative of four repeats. (**F**) Western blot showing uniquitination status of EGFP-STIL (wild type, WT, S76L mutant & S76L/S183A double mutant) transfected in MCF7 cells and immunoprecipitated using EGFP antibody. IgG bands serve as loading control. The blot is representative of two repeats. (**G**) Immunofluorescence images of S-phase synchronized MCF7 cells expressing EGFP (control) or EGFP-STIL

constructs. The cells were stained for Centrin-1 (centrosome marker) and DAPI (nuclear marker). Insets show a magnified view of the centrioles. Scale bar: 5μm. (**H**) Bar graph represents mean EGFP signals±SEM at centrosomes (CSs) in the respective conditions indicated in (G). Results are from four independent experiments (n=50-150). ∗∗∗∗$p<0.0001$ (two-tailed unpaired Student's t-test).

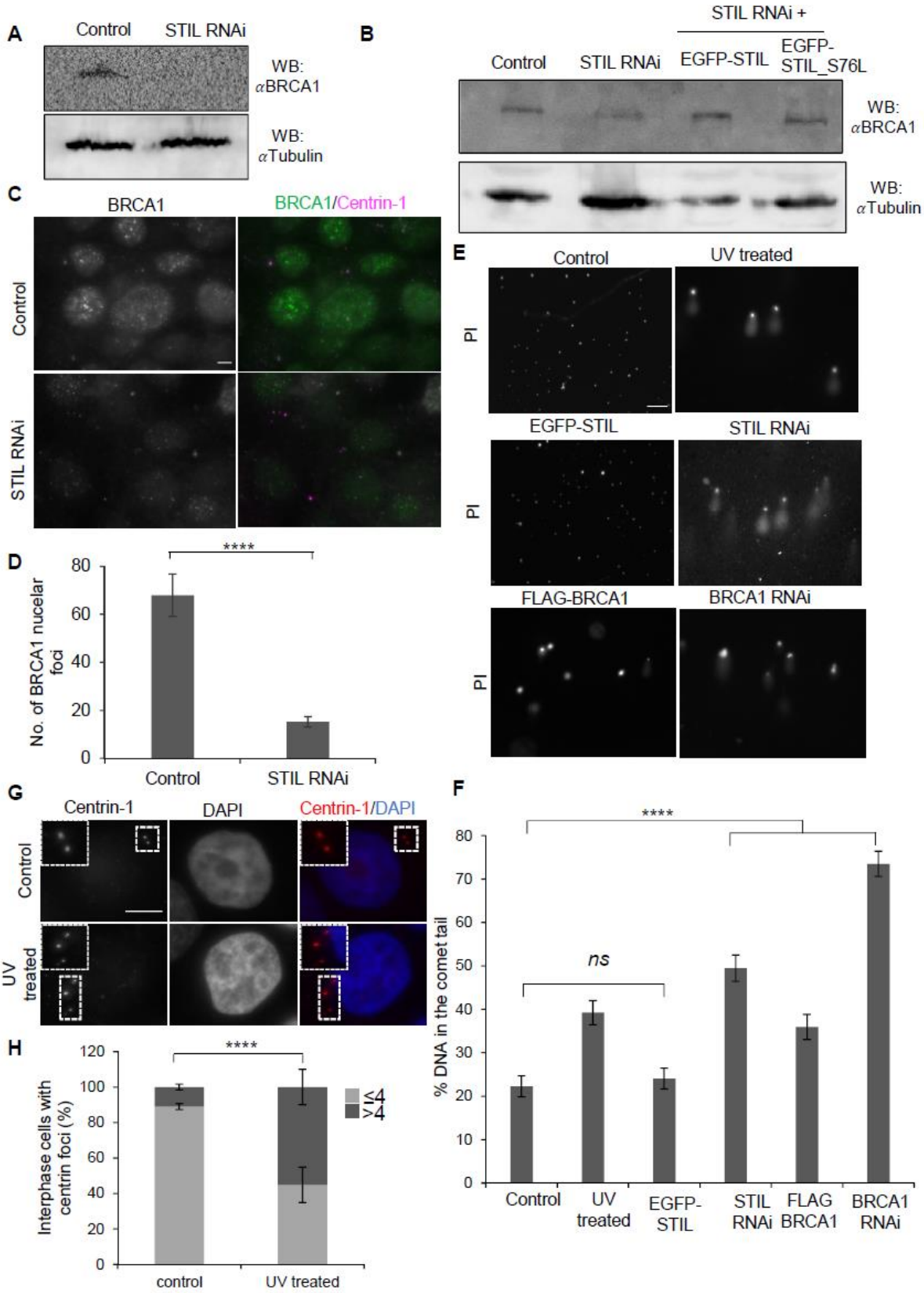
A
Control
STIL RNAi
WB: αBRCA1
WB: αTubulin
B
STIL RNAi +
Control
STIL RNAi
EGFP-STIL
EGFP-STIL_S76L
WB: αBRCA1
WB: αTubulin
C
BRCA1
BRCA1/Centrin-1
Control
STIL RNAi
D
No. of BRCA1 nucelar foci
****
Control
STIL RNAi
E
Control
UV treated
PI
EGFP-STIL
STIL RNAi
FLAG-BRCA1
BRCA1 RNAi
F
% DNA in the comet tail
****
ns
Control
UV treated
EGFP-STIL
STIL RNAi
FLAG BRCA1
BRCA1 RNAi
G
Centrin-1
DAPI
Centrin-1/DAPI
Control
UV treated
H
Interphase cells with centrin foci (%)
****
≤4
>4
control
UV treated

Figure 4: **STIL depletion reduces number of BRCA1 foci in the cell nucleus, which causes DNA damages and centrosome amplification**. (**A**) Western blot showing endogenous BRCA1 levels in the total cell lysates of MCF7 cells in control *vs.* STIL RNAi α-tubulin serves as loading control. The blot is representative of four repeats. (**B**) Western blot showing BRCA1 levels in the total cell lysates of MCF7 of control, STIL RNAi and STIL RNAi complemented with RNAi resistant EGFP-STIL or EGFP-STIL-S76L. α-tubulin serves as loading control. The blot is representative of two repeats. (**C**) Immunofluorescence images of MCF7 cells stained for endogenous BRCA1 and centrin-1 (centrosome marker). Scale bar: 5μm. (**D**) Bar graph showing the average number of BRCA1 foci per cell±SEM for control *vs.* STIL RNAi conditions. Results are from two independent experiments (n=70-100). ∗∗∗∗ $p<0.0001$ (Two-tailed unpaired Student's t-test). (**E**) Immunofluorescence images of MCF7 cells for comet assay and stained with propidium iodide (PI) to assess varying levels of DNA damage for different conditions. Scale bar: 100μm. (**F**) Bar graph showing the average percentage of DNA in comet tail±SEM as quantified from experiment (E). Results are from two independent experiments (n=150-250). ns, not significant ($p>0.05$); ∗∗∗∗$p<0.0001$ (Two-tailed unpaired Student's t-test). (**G**) Immunofluorescence images of S-phase synchronized MCF7 cells stained for centrin-1 (centriole marker) and DAPI (nuclear marker) in control and UV treated conditions. Insets show a

magnified view of centrioles. Scale bar: 5μm. (**H**) Bar graph showing the average percentage of interphase cells±SEM with >4 (dark gray) and 4 (light gray) centrin-1 dots for indicated conditions in (G). Results are from two independent experiments (n=80-100). ****p<0.0001 (Chi-squared test).

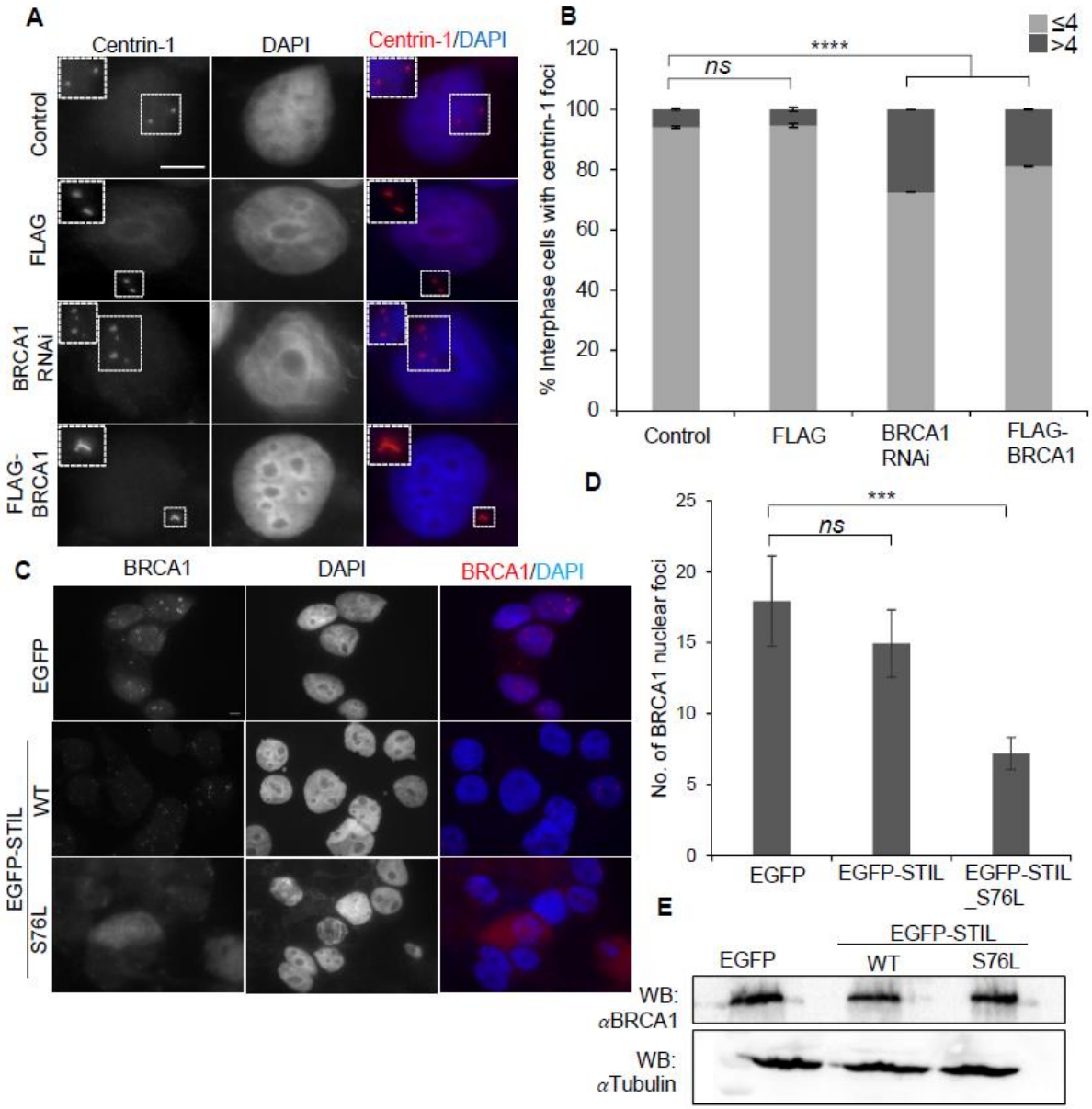

Figure 5: **BRCA1 regulate centrosome amplification and oncogenic STIL-S76L causes reduced nuclear foci of BRCA1**. (**A**) Immunofluorescence images for S-phase synchronized MCF7 cells stained for centrin-1 (centriole marker) and DAPI (nuclear marker). Insets show a magnified view of the centrioles. Scale bar: 5μm. (**B**) Bar graph showing the mean percentage

of interphase cells ±SEM with >4 (dark gray) and □4 (light gray) centrin-1 dots for indicated conditions in (A). Results are from two independent experiments (n=100-150). ns, not significant (p>0.05); ∗∗∗∗p<0.0001 (Chi-squared test). (**C**) Immunofluorescence images for S-phase synchronized MCF7 cells immunostained for endogenous BRCA1 and DAPI (nuclear marker) expressing EGFP, EGFP-STIL and EGFP-STIL-S76L. Scale bar: 5μm. (**D**) Bar graph showing the average number of BRCA1 nuclear foci ±SEM as quantified from (C). Results are from two independent experiments (n=70-100). ns, not significant (p>0.05); ∗∗∗p<0.001 (Two-tailed unpaired Student's t-test.) (**E**) Western blot showing endogenous BRCA1 levels in the total cell lysates of MCF7 cells expressing EGFP (control), EGFP-STIL (WT, wild type; S76L mutant). α-tubulin serves as loading control. The blot is representative of two repeats.

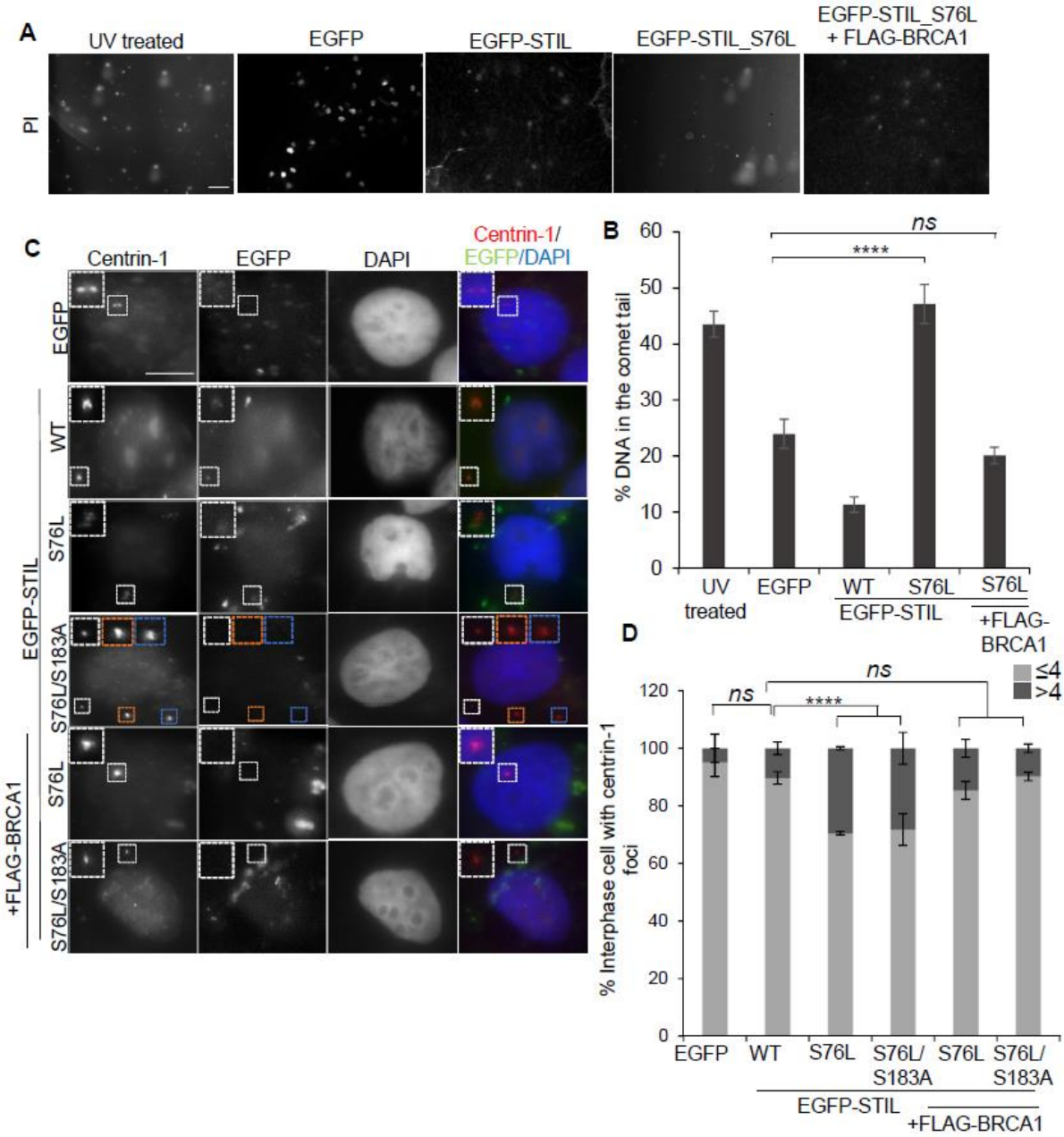

Figure 6: Exogenous BRCA1 rescues DNA damage and centrosome amplification phenotypes of oncogenic STIL-S76L. (**A**) Fluorescence images of MCF7 cells expressing EGFP (control), EGFP-STIL and EGFP-STIL-S67L with DNA stained with propidium iodide (PI) after

the comet assay. UV-treated MCF7 cells is a positive control. Scale bar: 100 μm. (**B**) Bar graph showing the averate percentage of DNA in the comet tails ±SEM as quantified from (A). Results are from two independent experiments (n=100-375). ns, not significant ($p>0.05$); ∗∗∗∗$p<0.001$ (Two-tailed unpaired Student's t-test). (**C**) Immunofluorescence images of S-phase synchronized MCF7 cells expressing indicated EGFP (control) and EGFP-STIL (WT, wild type; S76L mutant; S76L/S183A double mutant). Last two panels show cells co-expressing FLAG-BRCA1. The cells are stained for Centrin-1 (centriole marker) and DAPI (nuclear marker). Insets show a magnified view of the centrioles. Scale bar: 5μm. (**D**) Bar graph showing the mean percentage of interphase cells ±SEM with >4 (dark gray) and 4 (light gray) Centrin-1 dots as quantified from (C). Results are from two independent experiments (n=100-150) ns, not significant ($p>0.05$); ∗∗∗∗$p<0.0001$ (Chi-squared test).

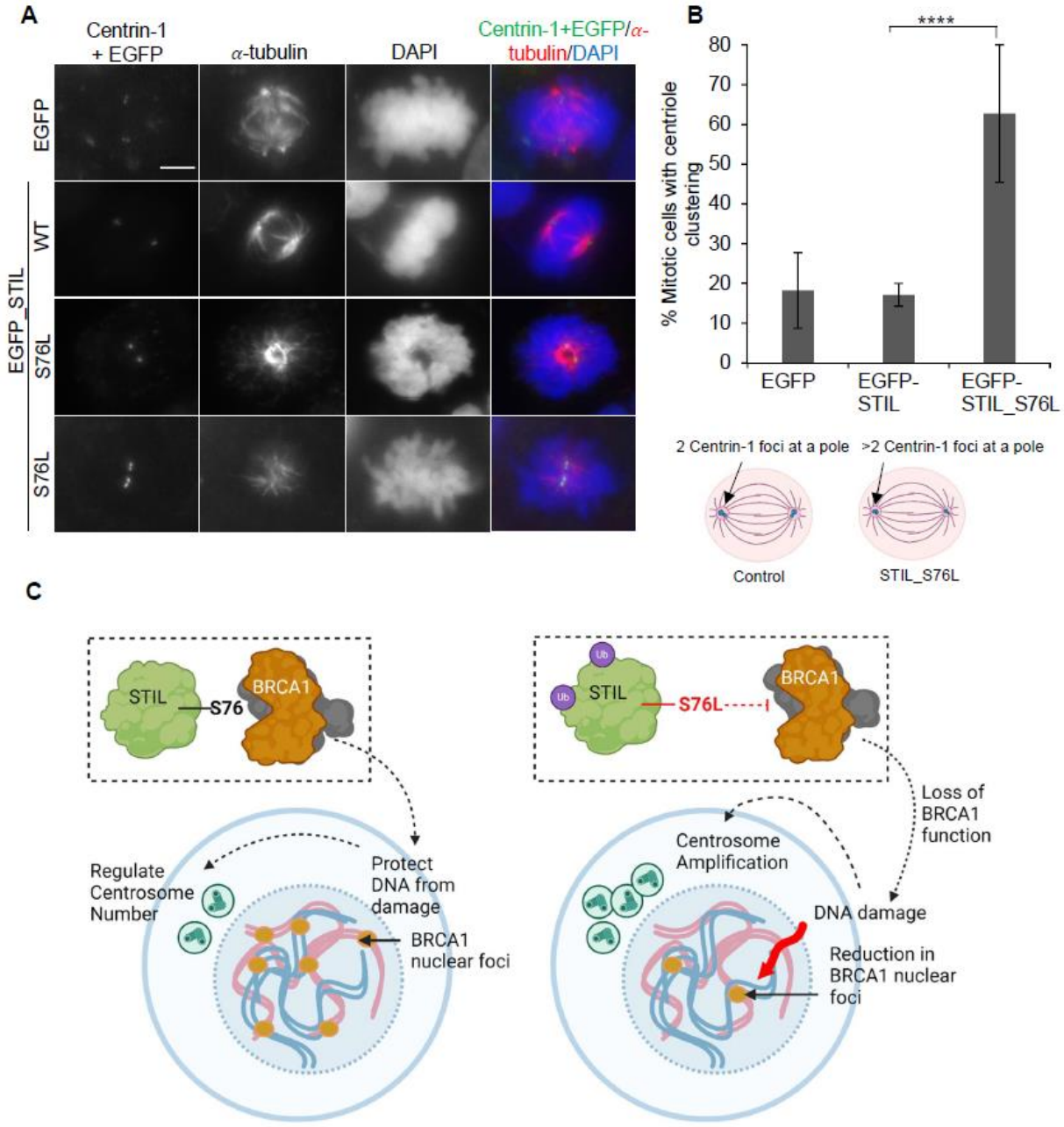

Figure 7: **Oncogenic STIL-S76L causes centrosome clustering**. (A) Representative images of M-phase synchronized MCF7 cells expressing EGFP (control), EGFP-STIL (WT, wild type; S76L mutant). The cells are immunostained with α-tubulin (red), centrin-1+EGFP signal (green), and

DAPI (blue). Scale bar: 5μm. (**B**) Bar graph representing average percentage (%) of mitotic cells with centriole clustering ±SEM for indicated condition in (A). The cartoon depicts that cells with more than two Centrin-1 dots per pole were regarded as centriole clustering. Results are from two independent experiments (n=30-40) ∗∗∗∗$p<0.0001$ (Chi-squared test). (**C**) The proposed model depicts that STIL interacts with BRCA1 and regulate DNA integrity by maintaining nuclear signals of BRCA1, which in turn is required for regulating centrosome number. In case of oncogenic STIL-S76L, interaction with BRCA1 is disrupted, which causes DNA damage and reduced BRCA1 signals in the nucleus, subsequently inducing centrosome amplification.

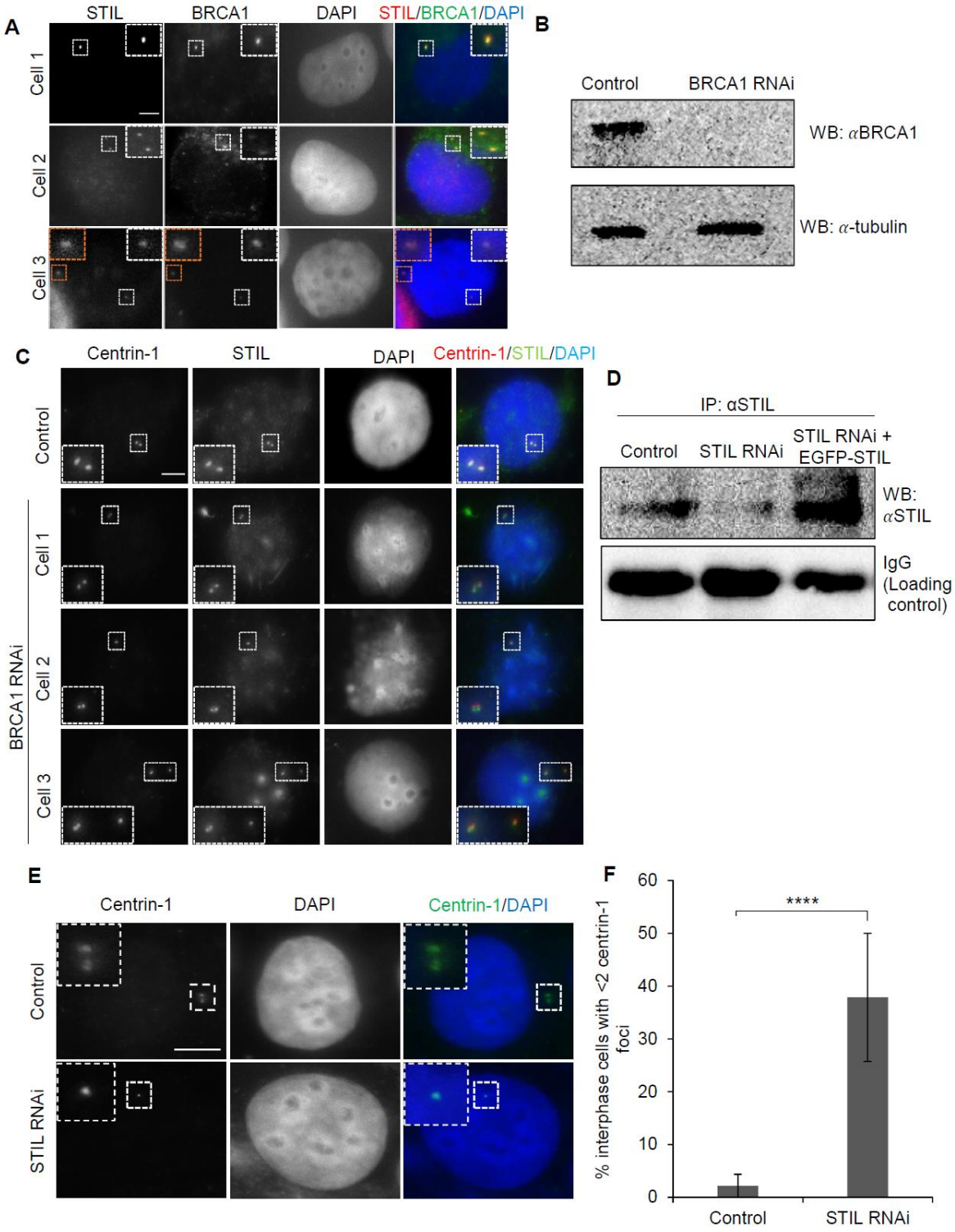
A
STIL
BRCA1
DAPI
STIL/BRCA1/DAPI
Cell 1
Cell 2
Cell 3
B
Control
BRCA1 RNAi
WB: αBRCA1
WB: α-tubulin
C
Centrin-1
STIL
DAPI
Centrin-1/STIL/DAPI
Control
BRCA1 RNAi
Cell 1
Cell 2
Cell 3
D
IP: αSTIL
Control
STIL RNAi
STIL RNAi + EGFP-STIL
WB: αSTIL
IgG (Loading control)
E
Centrin-1
DAPI
Centrin-1/DAPI
Control
STIL RNAi
F
% interphase cells with <2 centrin-1 foci
60
50
40
30
20
10
0
****
Control
STIL RNAi

Figure S1: (**A**) Immunofluorescence images of S-phase synchronized MCF7 cells stained for endogenous STIL & BRCA1. Insets show magnified view of centrioles. Scale bar: 5μm. (**B**) Western blot showing BRCA1 depletion after RNAi-treatment (72 nM) in the total cell lysate of MCF7 cells. α-tubulin serves as loading control. (**C**) Immunofluorescence images for S-phase synchronized MCF7 cells control *vs.* BRCA1 RNAi. Cells are stained for endogenous STIL, centrin-1 (centriole marker) and DAPI (nuclear marker). (**D**) Western blot showing immunoprecipitated (IP) STIL levels in control, STIL RNAi (72 nM, endogenous STIL depletion) and STIL RNAi+RNAi-resistant EGFP-STIL condition. IgG serves as a loading control. (**E**) Immunofluorescence images of S-phase synchronized MCF7 cells stained with Centrin-1 and DAPI. Insets show magnified view of centrioles. Scale bar: 5μm. (**F**) Bar graph showing the mean percentage of interphase cells ±SEMs with <2 Centrin-1 dots from the indicated conditions in (E). Results are from two independent experiments (n=60-70). ∗∗∗∗p<0.0001 (Chi-squared test).